separations

MDPI

Article

Study on the Preparation of Magnetic Mn–Co–Fe Spinel and Its Mercury Removal Performance

Jiawei Huang [1], Zhaoping Zhong [1,*], Yueyang Xu [1,2,3] and Yuanqiang Xu [1]

[1] Key Laboratory of Energy Thermal Conversion and Control of the Ministry of Education, Southeast University, Nanjing 210096, China; 220190482@seu.edu.cn (J.H.); xyy_gdhb@126.com (Y.X.); 13092320301@163.com (Y.X.)
[2] China Energy Science and Technology Research Institute Co., Ltd., Nanjing 210046, China
[3] State Key Laboratory of Clean and Efficient Coal-Fired Power Generation and Pollution Control, Nanjing 210046, China
* Correspondence: zzhong@seu.edu.cn

Abstract: In this study, the manganese-doped manganese–cobalt–iron spinel was prepared by the sol–gel self-combustion method, and its physical and chemical properties were analyzed by XRD (X-ray diffraction analysis), SEM (scanning electron microscope), and VSM (vibrating sample magnetometer). The mercury removal performance of simulated flue gas was tested on a fixed bed experimental device, and the effects of Mn doping amount, fuel addition amount, reaction temperature, and flue gas composition on its mercury removal capacity were studied. The results showed that the best synthesized product was when the doping amount of Mn was the molar ratio of 0.5, and the average mercury removal efficiency was 87.5% within 120 min. Among the fuel rich, stoichiometric ratio, and fuel lean systems, the stoichiometric ratio system is most conductive to product synthesis, and the mercury removal performance of the obtained product was the best. Moreover, the removal ability of Hg^0 was enhanced with the increase in temperature in the test temperature range, and both physical and chemical adsorption play key roles in the spinel adsorption of Hg^0 in the medium temperature range. The addition of O_2 can promote the removal of Hg^0 by adsorbent, but the continuous increase after the volume fraction reached 10% had little effect on the removal efficiency of Hg^0. While SO_2 inhibited the removal of mercury by adsorbent, the higher the volume fraction, the more obvious the inhibition. In addition, in an oxygen-free environment, the addition of a small amount of HCl can promote the removal of mercury by adsorbent, but the addition of more HCl does not have a better promotion effect. Compared with other reported adsorbents, the adsorbent has better mercury removal performance and magnetic properties, and has a strong recycling performance. The removal efficiency of mercury can always be maintained above 85% in five cycles.

Keywords: mercury removal; magnetic; manganese; cobalt; iron; spinel

Citation: Huang, J.; Zhong, Z.; Xu, Y.; Xu, Y. Study on the Preparation of Magnetic Mn–Co–Fe Spinel and Its Mercury Removal Performance. *Separations* **2021**, *8*, 225. https://doi.org/10.3390/separations8110225

Academic Editor: Attilio Naccarato

Received: 27 October 2021
Accepted: 17 November 2021
Published: 19 November 2021

1. Introduction

Mercury, as a highly toxic trace element in nature, has attracted wide attention from environmentalists all over the world due to its volatility and bioaccumulation [1–3]. It mainly exists in nature in the form of organic mercury, inorganic mercury, and metallic mercury [4]. In China, coal-fired power plants are the main source of mercury emissions, accounting for about 38% [5,6] of total mercury emissions. This situation has been highly valued by the Chinese government. The "Emission standard of air pollutants for thermal power plants" (GB13223-2011) issued in 2011 clearly stipulated that the mercury emission limit of coal-fired boilers was 30 $\mu g/m^3$ or less for the first time [7]. In addition, "the Minamata Convention on Mercury" signed by 128 countries and regions including China has also formally entered into force on 16 August 2017 [8]. In order to implement the green and sustainable development strategy and "the Minamata Convention on Mercury", the development of high-efficiency and low-cost coal-fired flue gas mercury removal

technology is urgently needed. Flue gas mercury is mainly composed of particulate mercury (Hg^P), oxidized mercury (Hg^{2+}), and elemental mercury (Hg^0). Among them, Hg^P can be removed by dust removal equipment, and Hg^{2+} is easily removed by wet desulfurization equipment, only Hg^0 is difficult to remove with existing control equipment [9–14]. At present, the more mainstream coal-fired flue gas mercury removal technology is still activated carbon injection (ACI) mercury removal technology, but this technology has disadvantages such as high price, poor recovery, and reduced fly ash quality, which limits its large-scale application [15–20]. Therefore, there is an urgent need to develop an efficient and easy-to-recover mercury removal adsorbent that can replace activated carbon.

In recent years, the research on non-carbon-based adsorbents can be divided into fly ash, mineral adsorbents, precious metals, metal oxides, and metal sulfides. Zhang et al. [17] studied the mercury removal performance of fly ash modified by $CaCl_2$, $CaBr_2$, and HBr, and the results showed that the mercury removal capacity of fly ash modified with different halogen compounds was significantly improved. Shi et al. [21] synthesized a new type of attapulgite catalyst (CeO_2/Atp (1:1)) that can maintain good catalytic activity in a wide temperature window, which can achieve a mercury removal efficiency of 97.75% at 200 °C. Cai et al. [15] studied the mercury removal performance of bentonite modified by KI and KBr, and the results showed that with the increase in the active material loading and the temperature (80–180 °C), the mercury removal efficiency increased, and compared with KBr modified, KI modified bentonite has better mercury removal performance. He et al. [22] synthesized Ce–Mn/Ti–PILC with a large specific surface area, which used a clay material similar to zeolite as the matrix. The results showed that under the HCl-free atmosphere, the 6%Ce–6%MnOx‖Ti–PILC catalyst could maintain a mercury removal efficiency above 90% in the range of 100–350 °C. After depositing silver nanoparticles on SBA–15, Xie et al. [23] prepared a silver-loaded SBA–15 adsorbent and found that mercury could form a silver amalgam with nano silver particles, and the mercury capture efficiency could reach 90% at 150 °C. Cimino et al. [24] developed two manganese-based catalysts for synergistic removal of NOx and Hg. The study found that the conversion of NOx and the removal of Hg were greatly affected by the type of carrier. TiO_2 is more suitable as a carrier for manganese oxide than Al_2O_3. Liu et al. [25] conducted a mercury adsorption performance test on the amorphous CoS synthesized by the liquid-phase precipitation method under the condition of 50 °C, and found that its adsorption capacity could reach 20.7 mg/g at a penetration rate of 25%. Li et al. [26] prepared nano ZnS with excellent mercury removal performance under high temperature conditions of 180 °C, and its adsorption capacity of Hg^0 at 50% transmission rate could reach 0.498 mg/g. Kong et al. [27] studied the change in mercury removal performance of CuO/TiO_2 and CuS/TiO_2 in the presence of SO_2 and H_2O, and the results showed that the mercury removal performance of CuO/TiO_2 was significantly reduced, while CuS/TiO_2 showed good resistance to H_2O and SO_2. Liu et al. [28] also showed that the mercury adsorption performance of CuS was hardly affected by SO_2 and H_2O. Although these non-carbon-based adsorbents have good mercury removal capacity, they are generally not easy to recycle, while magnetic adsorbents, which are easy to separate from fly ash, can be recycled and reused well, which can significantly reduce the operation cost of power plants.

At present, two common magnetic materials, γ–Fe_2O_3 and Fe_3O_4, are mainly used to modify the adsorbents [2,7,12,29,30], and then the modified adsorbents are separated from the fly ash by the magnetic separation method to realize their recycling. Although spinels containing MF_2O_4 (M = Co, Mn, Cu, Zn, Fe, Ni, Mg, etc.) with high catalytic activity and strong magnetic response have been widely used in other fields [31,32], the research on mercury removal from coal-fired flue gas is relatively rare. Liao et al. [11] synthesized an Fe–Ti–Mn spinel with excellent mercury removal performance, which can be regenerated after washing with water and heating at high temperatures. Xiong et al. [14] also showed that the Fe–Ti–Mn spinel had a good adsorption performance for Hg^0. The Mn–Fe spinel synthesized by Dang Hao [13] has good mercury removal performance in the temperature range of 50–100 °C, and it can be regenerated after being washed by acidic

NaClO solution. After five cycles of adsorption, it can still maintain more than 95% of Hg^0 mercury removal efficiency. In addition, it has been reported that Co-doped iron oxides can improve the adsorption capacity of Hg^0 [33,34]. Considering that Co is a natural ferromagnetic element, this study plans to dope manganese ions into cobalt ferrite spinel to prepare a magnetic manganese–cobalt–iron spinel, in order to achieve efficient mercury removal and recyclability of the adsorbent.

In this study, the magnetic spinel $Mn_xCo_{(1-x)}$ Fe_2O_4 (x = 0–1.0) was prepared by the sol–gel self-combustion synthesis method and characterized by XRD, SEM, and VSM. The adsorption performance of gas-phase zero-valent mercury (Hg^0) was investigated in a fixed-bed reaction system, and the effects of Mn doping amount, fuel addition amount, reaction temperature, and flue gas components on the mercury removal performance were discussed, and the regeneration performance of the screening of the sorbent was explored, aiming to provide theoretical guidance and research basis for the development of efficient and recyclable spinel ferrite adsorbents.

2. Materials and Methods

2.1. Materials

$(CH_3COO)_2Mn{\cdot}4H_2O$, $(CH_3COO)_2Co{\cdot}4H_2O$, $Fe(NO_3)_3{\cdot}9H_2O$, and citric acid ($C_6H_8O_7$) as well as the above chemical reagents were analytically pure; high-purity deionized water was used in the experiment.

2.2. Sample Preparation

Magnetic Mn–Co–Fe spinel was synthesized by the sol–gel auto-combustion method. Taking the preparation of $Mn_{0.5}Co_{0.5}Fe_2O_4$ as an example, the specific preparation method is as follows. First, 3.68 g $(CH_3COO)_2Mn{\cdot}4H_2O$, 3.74 g $(CH_3COO)_2Co{\cdot}4H_2O$, 24.24 g $Fe(NO_3)_3{\cdot}9H_2O$, and 9.61 g citric acid were dissolved in a proper amount of deionized water. The molar ratio of Mn^{2+}, Co^{2+}, and Fe^{3+} was 1:1:4, and the ratio of the total oxidation value (O) of the oxidant (ferric nitrate) to the total reduction value (F) of the fuel (citric acid) was the stoichiometric ratio 1 (O/F = 1). After stirring for 30 min, the mixture was placed in a magnetic water-bath stirring pot at 70 °C for evaporation and stirring to remove water, and a wet gel was obtained. The obtained wet gel was dried and milled at 100 °C, and then put into a muffle furnace that had been preheated to 400 °C for the reaction. After the reaction was completed, the obtained product was calcined in a muffle furnace that had been preheated to 500 °C for 4 h. Finally, the obtained sample was placed in a drying dish for later use and recorded as 1M1C-1.

In the same way, $CoFe_2O_4$, $Mn_{0.25}Co_{0.75}Fe_2O_4$, $Mn_{0.75}Co_{0.25}Fe_2O_4$, and $MnFe_2O_4$ were prepared by changing the amount of Mn doping, which were denoted as CFO-1, 1M3C-1, 3M1C-1, and MFO-1 respectively. By changing the amount of fuel added, $Mn_{0.5}Co_{0.5}Fe_2O_4$ (O/F = 0.5), $Mn_{0.5}Co_{0.5}Fe_2O_4$ (O/F = 0.75), $Mn_{0.5}Co_{0.5}Fe_2O_4$ (O/F = 1.25), and $Mn_{0.5}Co_{0.5}Fe_2O_4$ (O/F = 1.5) were prepared as 1M1C-0.5, 1M1C-0.75, 1M1C-1.25, and 1M1C-1.5, respectively.

2.3. Characterization of Samples

A D8 ADVANCE X-ray diffractometer (Bruker, Germany) was used to detect and analyze the composition of the sample, and the sample was scanned at 5–90°; a Hitachi SU800 scanning electron microscope (Hitachi, Japan) was used to observe the microstructure of the product, and the particle size and particle size distribution of the sample were characterized by the image analysis method. The samples were analyzed for magnetic responsiveness and separability using a PPMS–9 (VSM) integrated physical property measurement system (Quantum Design, San Diego, CA, USA).

2.4. Experimental Device

The mercury removal performance of $Mn_xCo_{1-x}Fe_2O_4$ spinel adsorbents was tested by a fixed-bed experimental device, which includes a gas distribution section, a mercury generator, a fixed-bed reactor, a mercury analyzer, and a waste gas treatment. The schematic

diagram of the experimental device is shown in Figure 1. The gas distribution was provided by a compressed gas cylinder. The gas was accurately controlled by a mass flow meter and the total flow rate of the gas was kept at 1 L/min. A total of 200 mL/min of N_2 was used as a carrier gas to be introduced into the mercury permeation tube, and gaseous Hg^0 was introduced into a gas mixing chamber. N_2 (balance gas), O_2, SO_2, and HCl gases from the gas distribution system and mercury vapor were fully mixed in the gas mixing chamber to simulate coal-fired flue gas. Before the experiment, the gas flow was switched to the bypass of the reaction tube, and the initial mercury concentration in the flue gas was measured by a VM3000 mercury detector (MI Company, Germany). After the mercury source was stable, the gas flow was switched to the main path, and the simulated flue gas containing mercury passed through the adsorbent for the mercury removal experiment. The mercury concentration in the flue gas at the outlet of the reaction tube was recorded in real time by the VM3000. The time of each test was 120 min. The tail gas discharged during the experiment was absorbed by activated carbon to prevent environmental pollution. Except for the quartz reaction tube, all connecting pipes are made of polytetrafluoroethylene, and the corresponding pipes were heated and controlled with heating belts to prevent mercury vapor from depositing on the inner wall of the pipes. During the experiment, the balance gas N_2 was 800 mL/min. When other gases are added, the corresponding balance gas should be reduced. The initial mass concentration of mercury (Hg^0) was constant at (85 ± 0.5) μg/m^3, and the adsorbent dosage was 50 mg (passing through a 200-mesh sieve). The mercury removal efficiency (η) is defined as shown in Equation (1), where c_{in} and c_{out} represent the mass concentrations of Hg at the reactor inlet and outlet (μg/m^3), respectively.

$$\eta = (1 - c_{out}/c_{in}) \times 100\% \quad (1)$$

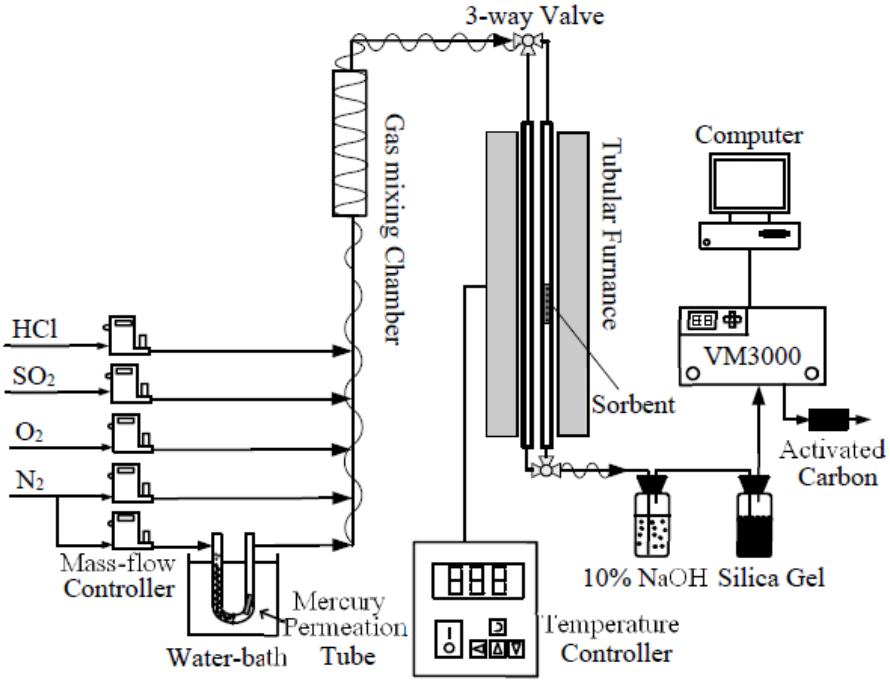

Figure 1. Sketch diagram of the mercury removal experimental apparatus.

3. Results and Discussion

3.1. Sample Characterization Analysis

3.1.1. XRD Analysis

Figure 2 shows the XRD diffractogram of spinels prepared with different doping amounts of Mn. It can be seen from Figure 2 that the main diffraction peaks in all spinel XRD diffractograms were basically consistent with the standard diffractogram of maghemite (γ–Fe_2O_3) (JCPDS: 39–1346) and appeared at 18.28, 30.22, 35.48, 37.32, 43.16, 53.90, 57.10, and

62.70° corresponding to the diffraction planes (111), (220), (311), (222), (400), (422), (511), and (440), respectively. In addition, except for the characteristic peak of Mn_2O_3(JCPDS: 41–1442) appearing at 55.22° and corresponding to the diffraction plane (440) in MFO-1, there were no characteristic peaks of cobalt and manganese oxides in the remaining spinels, which means that for CFO-1, 1M3C-1, 1M1C-1, and 3M1C-1, the cobalt and manganese ions had been completely doped into the spinel structure. As far as MFO-1 is concerned, manganese ions were not fully incorporated, and a small amount of 6.04% Mn_2O_3 phase impurities were generated. In addition, it can be seen that, except for 1M1C-1, the characteristic peaks of α–Fe_2O_3(JCPDS: 89–0596) appearing at 33.02, 49.96 and 64.00° and corresponding to the diffraction planes (104), (024), and (300), respectively, appeared in the rest of the spinels. There were 8.74% and 9.20% α–Fe_2O_3 phase impurities in CFO-1 and 1M3C-1, respectively, 17.09% in 3M1C-1, and 37.96% in MFO-1.

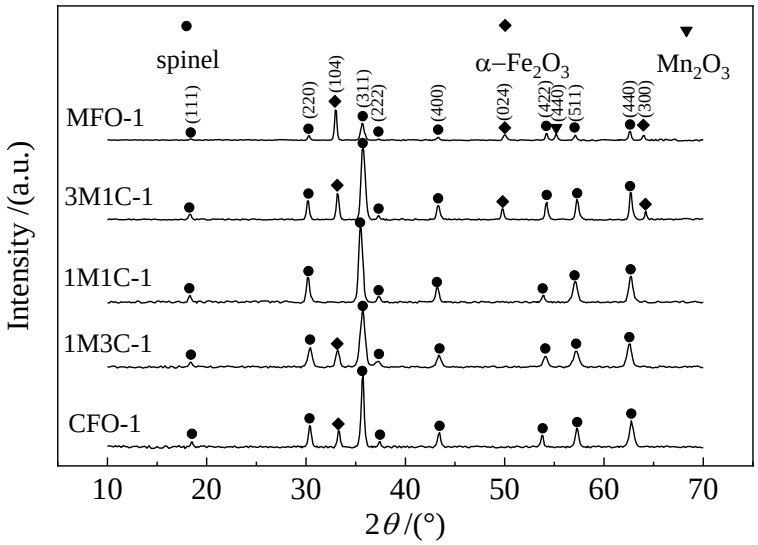

Figure 2. XRD patterns of the $Mn_xCo_{1-x}Fe_2O_4$ spinels.

Figure 3 shows the XRD diffractogram of the spinel prepared with different amounts of fuel. It can be seen from Figure 3 that the $Mn_{0.5}Co_{0.5}Fe_2O_4$ spinels prepared under different fuel addition amounts all belonged to a single-phase spinel structure, and no other impurity phases were generated. Compared with 1M1C-0.5 and 1M1C-1.5, the diffraction peak of 1M1C-1 was sharper and the peak intensity greater, which indicates that the crystallinity of 1M1C-1 was higher. According to the Scherrer formula shown in Equation (2), the average grain sizes of 1M1C-0.5, 1M1C-1, and 1M1C-1.5 were 17.67 nm, 21.21 nm, and 13.26 nm, respectively. It can be seen that the rich-burn and lean-burn systems are not conducive to grain growth. Only the stoichiometric ratio system is most conducive to product formation and grain growth, which is consistent with the results reported in the literature [35,36].

$$D = K\lambda / \beta \cos\theta \quad (2)$$

where D is the size of the crystal grain (nm); K is the shape factor of the particle, generally 0.9; λ is the X-ray wavelength used in the test, 0.1542 nm in this paper; β is the maximum half-width of the diffraction peak; and θ is the diffraction angle corresponding to the X-ray diffraction peak.

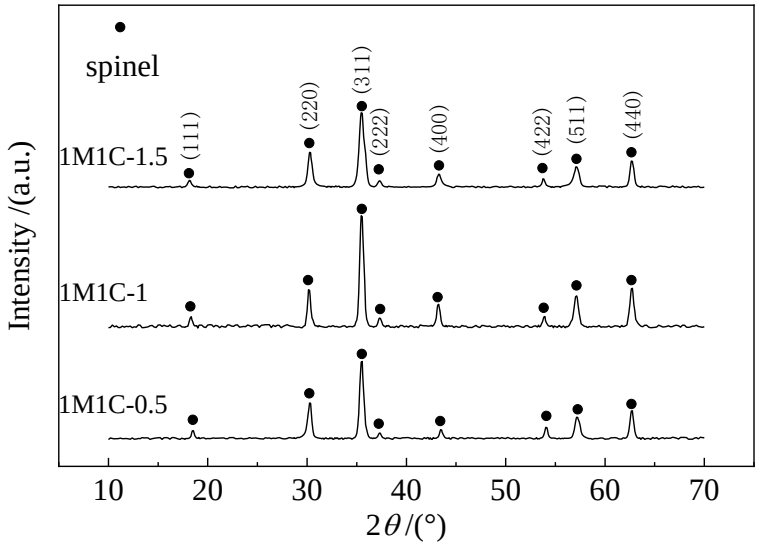

Figure 3. XRD patterns of spinels obtained with different fuel dosages.

3.1.2. SEM Analysis

Figure 4 shows the particle size distribution and SEM micrographies of the 1M1C-1, 3M1C-1, and MFO-1 spinels. We could see from Figure 4 that the particle size distribution of 1M1C-1 was relatively narrow, and the particle size was smaller. According to statistical calculations, the smallest particle size was 66 nm, the largest particle size was 1.52 μm, and the average particle size was 370 nm. Combined with the SEM micrographies, it can be seen that the particles were all spherical granular aggregates, conforming to the characteristics of an equiaxed crystal system, indicating that the synthesized product had a single-phase spinel structure. The minimum particle size of 3M1C-1 was 90 nm, the maximum particle size was 1.37 μm, and the average particle size was 381 nm. Compared to 1M1C-1, the particles of 3M1C-1 tended to be of medium size, and the average particle size increased slightly. Combined with the SEM micrographies, it can be seen that there are flaky particles in the product, which conform to the characteristics of a hexagonal crystal system. This shows that the impurity of α–Fe_2O_3 appeared in the sample. At the same time, it is easy to learn that the minimum particle size of MFO-1 was 108 nm, the maximum particle size was 2.11 μm, and the average particle size was 388 nm. Compared with 3M1C-1, the particles of MFO-1 were more closed to larger particles. Combined with the SEM micrographies, it can be seen that the obvious secondary agglomeration phenomenon could be observed in the product, and relatively more flaky particles could be found.

3.1.3. VSM Analysis

Figure 5 shows the hysteresis loops of 1M1C-1, 3M1C-1, and MFO-1 spinels, which shows that 1M1C-1, 3M1C-1, and MFO-1 spinels all had superparamagnetism and could be spontaneously magnetized under the action of an external magnetic field. Magnetic agglomeration will not occur during the demagnetization process, and the specific saturation magnetization was 41 emu/g, 19.25 emu/g, and 10.43 emu/g, respectively, which is consistent with the analysis results of XRD and SEM. The decrease in specific saturation magnetization is due to the formation of α–Fe_2O_3 impurity, and the higher the impurity ratio, the greater the decrease. According to the literature [2], these three spinels can be attracted by magnets, but it can also be seen from Figure 5 that the required external magnetic field to achieve the same specific saturation magnetization of 1M1C-1 was the smallest, followed by 3M1C-1, and MFO-1 was the largest. Taking 10 emu/g as an example, MFO-1 needs an external magnetic field of 9000 Oe, 3M1C-1 only needs 1750 Oe, and 1M1C-1 only needs 500 Oe. Therefore, from the perspective of engineering application, 1M1C-1 has better magnetic separation characteristics.

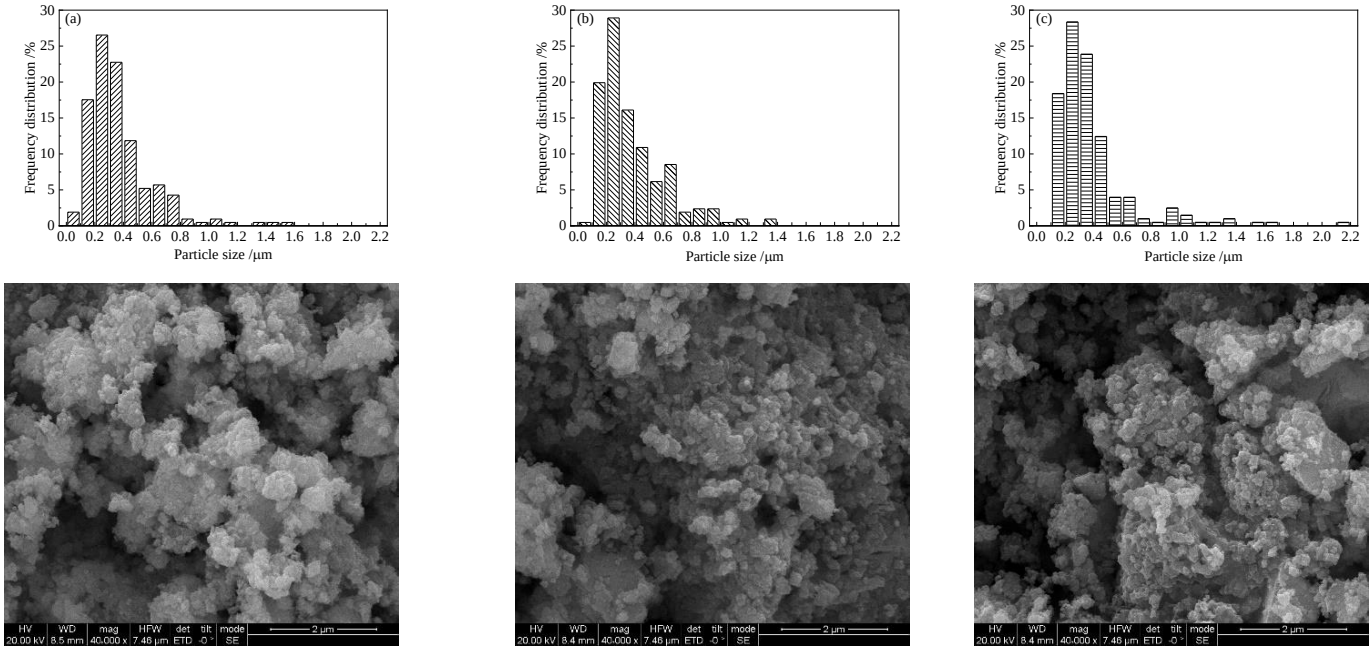

Figure 4. Particle size distributions and SEM micrographies of the spinel samples. (**a**) 1M1C-1; (**b**) 3M1C-1; (**c**) MFO-1.

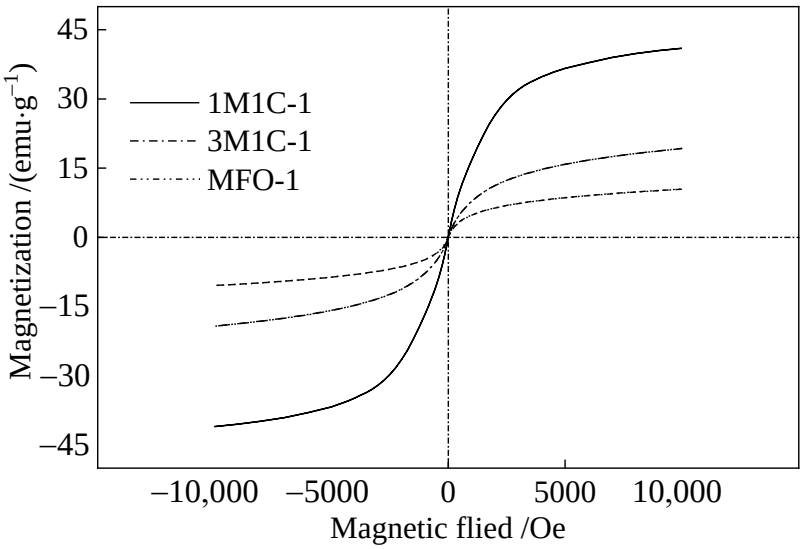

Figure 5. Hysteresis loop diagrams of three spinels.

3.2. Sorbent Mercury Removal Experiment

3.2.1. Influence of Different Doping Amount of Mn on the Performance of Mercury Removal

In order to study the effect of Mn doping on mercury removal by spinel adsorbent, this research applied five types of spinels obtained in the experiment to a fixed bed mercury adsorption experiment to test their mercury removal performance. The reaction temperature in the experiment was 150 °C. The flue gas atmosphere was pure N_2. The experimental results are shown in Figure 6.

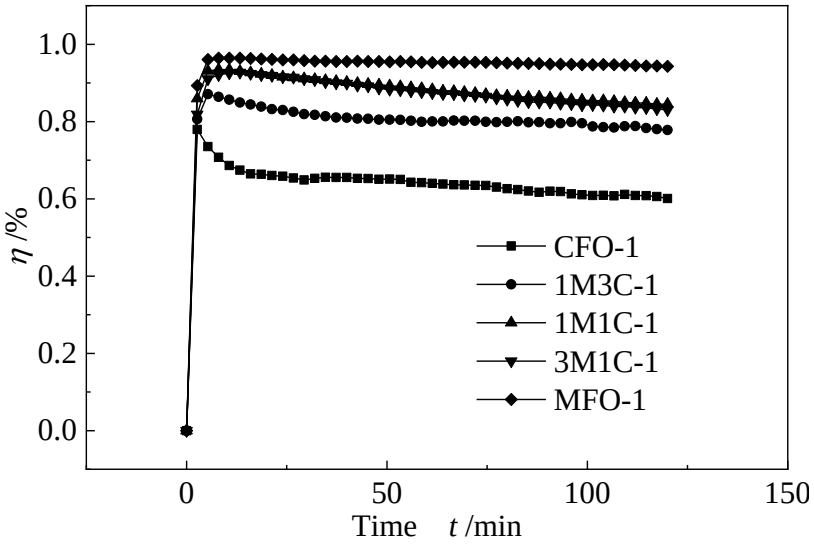

Figure 6. Effect of Mn doping content on the mercury removal efficiency of the adsorbent.

It can be seen from Figure 6 that the CFO-1 sample without Mn reached the highest mercury removal efficiency of 77.9% at the beginning, and then began to decline continuously, with an average mercury removal efficiency of 63.7% within 120 min. When the molar ratio of Mn was 0.25, the 1M3CFe sample initially reached a mercury removal efficiency of 80.6%, and a small increase occurred in a short period of time thereafter, reaching the highest mercury removal efficiency of 87.1%, and then began to slowly decrease. The average mercury removal efficiency during the test period was 80%, which shows that the doping of a small amount of Mn can greatly increase the mercury removal efficiency of the cobalt ferrite spinel on one hand, and on the other hand, can prolong the effective action time of the adsorbent. When the Mn doping amount is further increased to 0.5 by mole ratio, the initial, maximum, and average mercury removal efficiency of 1M1C-1 increased to 86%, 93.5%, and 87.5%, respectively, and the increase rates were 6.7%, 7.3%, and 9.4%, respectively. This shows that the downward trend of mercury removal efficiency had greatly slowed down, and the overall high-efficiency action time was further increased. When the molar ratio of Mn doping was 0.75, the mercury removal efficiency of 3M1C-1 dropped by 4.8%, 0.9%, and 1%, respectively, indicating that the formation of α–Fe_2O_3 impurity makes the absolute content of high-efficiency mercury removal active ingredients in the same mass adsorbent. The decrease resulted in a slight decrease in the mercury removal efficiency when the Mn doping amount increased. When Mn was fully doped, the initial, highest and average mercury removal efficiency of the MFO-1 samples were 89.3%, 96.4%, and 94.2%, respectively, indicating that the mercury removal efficiency of MFO-1 dropped very slowly after rising to its highest, and almost remained unchanged. At the same time, it also showed that the Fe–Mn spinel had very good mercury removal performance. In the case of generating more α–Fe_2O_3 impurities, it could still maintain a high mercury removal efficiency. It can be found that Mn-doped cobalt ferrite spinel had a good ability to remove Hg^0. As the Mn doping amount gradually increased from 0 to 0.5 in molar ratio, the mercury removal performance and high-efficiency action time gradually increased. However, when the doping amount reached a molar ratio of 0.75, the mercury removal efficiency of the adsorbent was slightly reduced, and the magnetic separation performance was also weakened. Even when the Mn was completely doped, the mercury removal efficiency of the adsorbent was again slightly improved. However, its magnetic separation performance was greatly reduced. In order to ensure the mercury removal performance and magnetic separation performance of the adsorbent at the same time, a molar ratio of 0.5 was taken as the best Mn doping amount.

3.2.2. The Effect of Different Fuel Addition on the Performance of Mercury Removal

In the case that the optimal doping amount of Mn was a 0.5 in molar ratio, in order to further study the influence of different fuel addition on the mercury removal performance of the prepared spinel, the mercury removal performance of the $Mn_{0.5}Co_{0.5}Fe_2O_4$ spinel prepared under the rich combustion, stoichiometric ratio, and lean-burn system was tested through fixed bed mercury adsorption experiments. The reaction temperature in the experiment was 150 °C, and the flue gas atmosphere was pure N_2. The experimental results are shown in Figure 7.

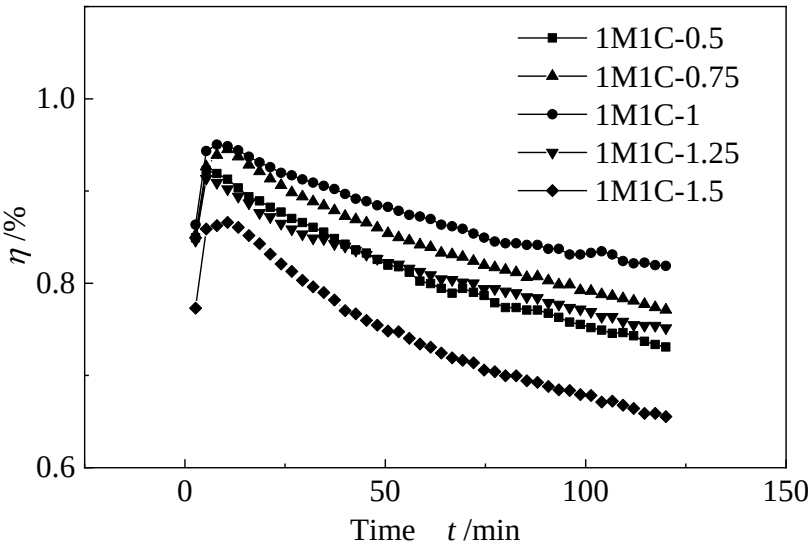

Figure 7. Effect of fuel addition content on the mercury removal efficiency of the adsorbent.

It can be seen from Figure 7 that when the Mn doping amount was 0.5 in molar ratio, the spinels prepared under different fuel addition amounts had relatively good mercury removal performance, and the relatively worst 1M1C-1.5 sample also had a 73.6% average mercury removal efficiency. Among them, the spinel prepared under the stoichiometric system had the best mercury removal performance, which is attributed to the fact that the stoichiometric system is most conducive to product formation and grain growth. For the rich combustion system, the oxidizer cannot provide the O required for the complete combustion of the fuel, and more O needs to be obtained from the surrounding environment. In the process of sample synthesis, NO^{3-} cannot completely oxidize the surrounding organic matter, and the heat released during oxidation is provided to the unreacted remaining organic matter in addition to heating the reaction system to react with external oxygen, and the reaction has some issues such as high initial temperature and slow reaction rate. It also showed that the fuel-rich system is not conducive to the formation of products, which explains the reason for η(1M1C-1) > η(1M1C-0.75) > η(1M1C-0.5). For the lean-burn system, the factor restricting the synthesis of the sample is the fuel. The heat released during oxidation cannot make the system reach the most suitable temperature for product formation. Therefore, the lean-burn system is not conducive to product formation, which explains the reason for η(1M1C-1) > η(1M1C-1.25) > η(1M1C-1.5). It can be found that in a fuel-rich system, reducing the amount of fuel added can improve the mercury removal performance of the prepared spinel. Similarly, in the lean-burn system, increasing the amount of fuel added will also increase the average mercury removal efficiency of the prepared spinel. In other words, the closer the O/F ratio is to 1, the better the mercury removal performance of the prepared spinel. According to the XRD analysis results, the products obtained under different systems are all single-phase spinel structures, and the magnetic separation performance should be similar. Therefore, to ensure the best mercury removal performance, O/F = 1 is the best fuel addition. All subsequent studies on other influencing factors have taken 1M1C-1 as the research object.

3.2.3. The Effect of Reaction Temperature on the Performance of Mercury Removal

In order to study the influence of temperature on the mercury removal effect of magnetic manganese–cobalt–iron spinel, the temperature of the fixed-bed reactor was set to 100 °C, 125 °C, 150 °C, 175 °C, and 200 °C, and the mercury removal experiment was carried out. The research object selected in the experiment was 1M1C-1, and the flue gas atmosphere was pure N_2. Figure 8 shows the mercury removal efficiency curve of 1M1C-1 at different reaction temperatures. It can be seen from Figure 8 that the Hg^0 removal efficiency of 1M1C-1 gradually increases with the increase in temperature. When the reaction temperature is 200 °C, the mercury removal efficiency was the highest, which was 90.1%. Across the entire reaction temperature range, 1M1C-1 could maintain good mercury removal performance, and there was an average mercury removal efficiency of 82.3% at 100 °C, indicating that the reaction temperature had relatively little effect on its mercury removal performance. In addition, it can be found that when the reaction temperature was increased from 100 °C to 125 °C, the increase in mercury removal efficiency was relatively small. From 125 °C to 150 °C and then to 175 °C, the increase in mercury removal efficiency was relatively large. However, from 175 °C to 200 °C, the increase in mercury removal efficiency weakened again. This is because the mercury adsorption process is the result of the combined effect of physical adsorption and chemical adsorption [10,37]. When the temperature was low (100–125 °C), the chemical adsorption was not obvious, and the physical adsorption was dominant. The effect of mercury removal performance was small. When the temperature rose (125–175 °C), chemical adsorption began to take effect, and the mercury removal performance was relatively greatly improved. When the temperature continued to rise (175–200 °C), physical adsorption began to be suppressed, and mercury desorption began to appear on the surface. Therefore, the improvement trend of the mercury removal performance slowed down. Based on the above analysis, in the following study, in order to highlight the effect of flue gas components on the mercury removal performance, 150 °C was selected as the benchmark experimental condition.

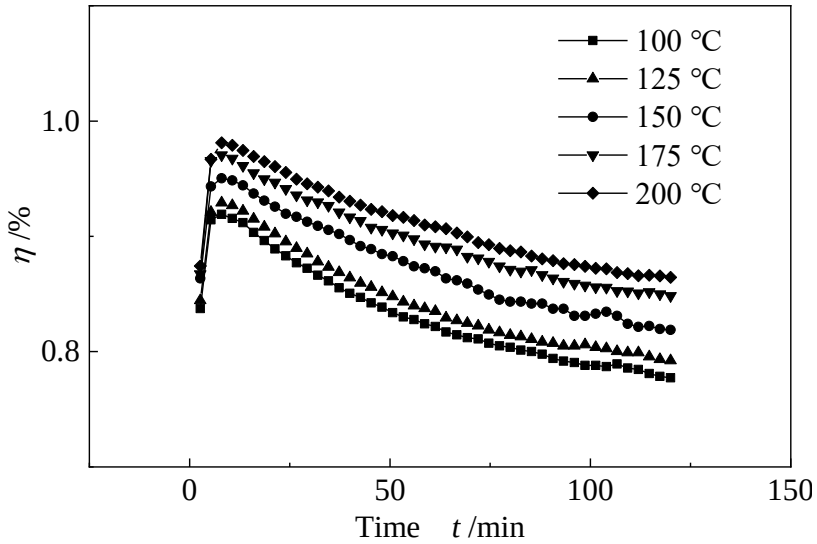

Figure 8. Effect of reaction temperature on the mercury removal efficiency of 1M1C-1.

3.2.4. Influence of Flue Gas Components on the Performance of Mercury Removal
Impact of O_2

Since different components (O_2, SO_2, HCl, etc.) in the flue gas will affect the mercury removal performance of the adsorbent, it is necessary to investigate the effect of different concentrations of O_2, SO_2, and HCl, on the mercury removal effect of the spinel. Figure 9 shows the effect of different volume fractions of O_2 on the removal of Hg^0 by 1M1C-1. It can be seen from the figure that without O_2, the mercury removal efficiency of 1M1C-1 showed a downward trend with the extension of the reaction time. When 5% O_2 was

introduced into the atmosphere, the downward trend of mercury removal efficiency was obviously curbed. The average mercury removal efficiency was significantly increased to 91.1%, and the volume fraction of O_2 continued to increase to 10%. The downward trend was further slowed down, and the average mercury removal efficiency was also further increased to 94.2%, indicating that O_2 plays a positive role in the removal of Hg^0. It can provide abundant active oxygen, and supplement the lattice oxygen consumed in the adsorption process or chemically adsorbed oxygen, thereby promoting the Hg^0 removal process [6,33,37,38]. However, when the O_2 volume fraction was further increased to 15%, the Hg^0 removal efficiency was basically not improved, indicating that 10% O_2 is sufficient to regenerate the lattice oxygen or chemisorption oxygen consumed on the surface.

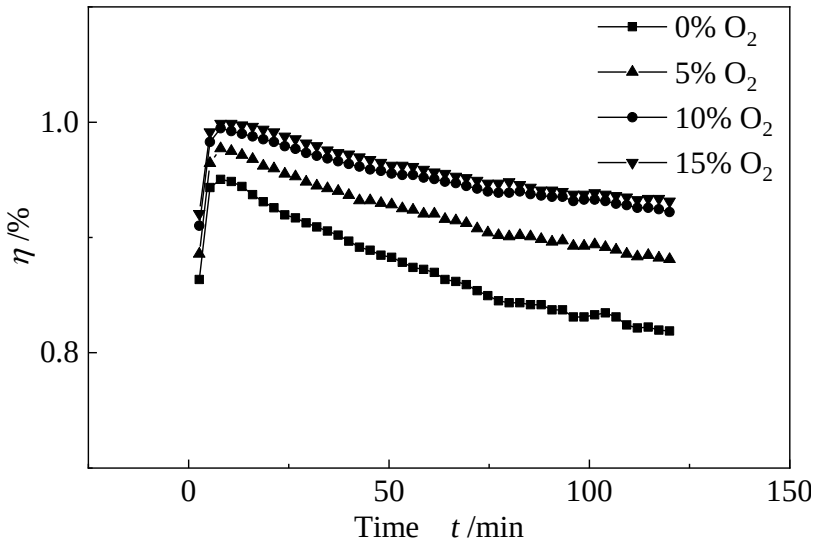

Figure 9. Effect of O_2 on the mercury removal efficiency of 1M1C-1.

Impact of SO_2

Figure 10 shows the effect of different volume fractions of SO_2 on the mercury removal performance of 1M1C-1. It is easy to see that after adding 0.04% SO_2 on the basis of pure N_2, the Hg^0 removal efficiency at the initial stage of adsorption had a slight increase, but after reaching the highest mercury removal efficiency, it dropped quickly, and the average mercury removal efficiency decreased compared to a pure N_2 atmosphere by 9%. The reason may be as shown in reactions (3)–(5) (O* is the surface active oxygen of the adsorbent) [11,39]. SO_2 molecules are more likely to occupy surface active sites. In the initial stage of adsorption, the preferentially adsorbed SO_2 molecules react with adsorbed Hg^0 to generate $HgSO_4$, which promotes the adsorption of Hg^0. However, the continuous introduction of SO_2 will occupy part of the active sites on one hand, and on the other hand, it may consume lattice oxygen or chemically adsorbed oxygen and react with metal oxides to form metal sulfates, occupy the surface, or block the pores, making the mercury removal efficiency decline faster. When the volume fraction of SO_2 continued to increase to 0.08% and 0.12%, the average mercury removal efficiency also continued to dropped to 74.5% and 70.7%. Therefore, different volume fractions of SO_2 have an inhibitory effect on 1M1C-1 mercury removal, and the higher the volume fraction, the more obvious the inhibitory effect. The reason may be the occurrence of competitive adsorption and side reactions [2,40].

$$SO_2(g) + 1M1CFe(surface) \rightarrow SO_2(ad) \quad (3)$$

$$SO_2(ad) + O^* \rightarrow SO_3(ad) \quad (4)$$

$$Hg^0(ad) + SO_3(ad) + O^* \rightarrow HgSO_4(ad) \quad (5)$$

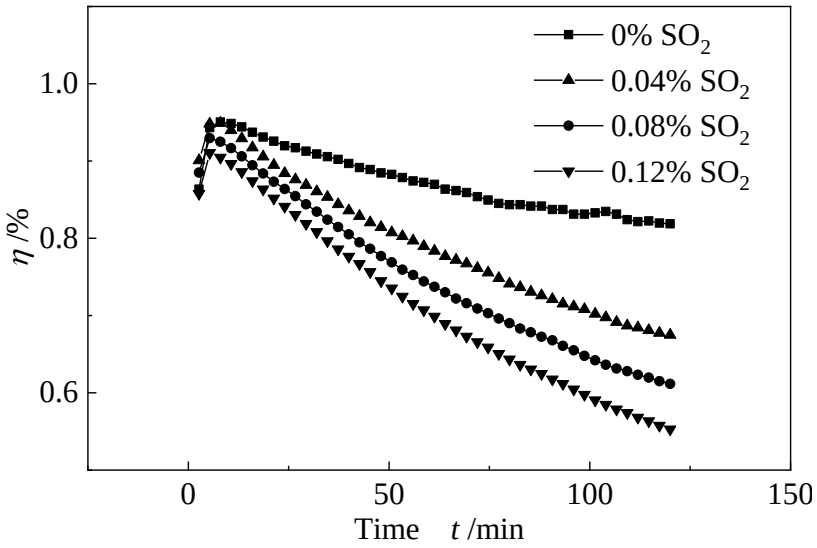

Figure 10. Effect of SO_2 on the mercury removal efficiency of 1M1C-1.

Compared with the side reactions, competitive adsorption accounts for a heavier proportion of the inhibition. Therefore, in order to further understand the competitive adsorption behavior of SO_2 on the surface of 1M1C-1, a mercury pre-adsorption experiment was carried out, as shown in Figure 11. In this experiment, first, we pre-adsorbed 1M1C-1 in Hg^0-containing N_2 for 120 min, then the mercury source was cut off and the total flue gas flow was kept constant. When the Hg^0 concentration in the flue gas was reduced to 0 μg/m^3, we added 0.12% SO_2 to the flue gas. It can be seen that the Hg^0 concentration in the flue gas rapidly increased to 20.1 μg/m^3, and then gradually decreased to 0 μg/m^3. This indicates that the introduction of SO_2 into the reaction system will cause the desorption of the weakly adsorbed mercury on the surface of the adsorbent, indicating that SO_2 and Hg^0 are competitively adsorbed during the removal of Hg^0 by 1M1C-1.

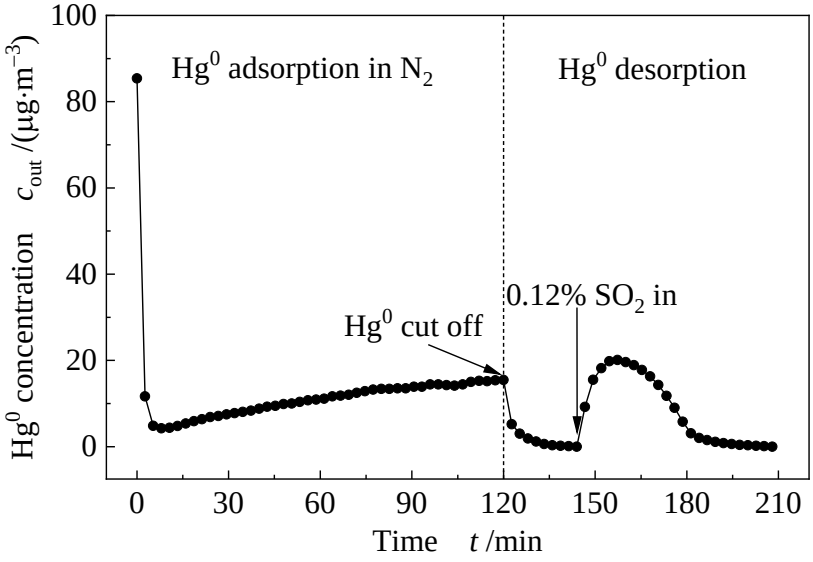

Figure 11. Effect of SO_2 on the desorption of mercury on 1M1C-1.

Impact of HCl

Figure 12 shows the effect of different volume fractions of HCl on the mercury removal performance of 1M1C-1. We could see that after 0.001% HCl was introduced into the reaction system, the average mercury removal efficiency increased by 3.4% to 89.3%, indicating that the addition of a small amount of HCl has a promoting effect on the

mercury removal of 1M1C-1. Because it is difficult for Hg^0 to directly react with HCl under a N_2 atmosphere and lower temperature, it is speculated that Mn^{4+} exists in the adsorbent and the reaction of Equations (6)–(8) occurs [3,29,41]. First, HCl is adsorbed on the surface of the adsorbent by separation and adsorption to form O–H bonds and Mn–Cl bonds, and the electrons of Mn^{4+} become Mn^{3+}, and the electrons lost by chloride ions become active chlorine atoms, and then the active chlorine atoms and the adsorbed state Hg^0 reacted to generate HgCl, which in turn generated $HgCl_2$. When the HCl volume fraction increased to 0.003%, the mercury removal efficiency only increased to 90.7%, and when it increased to 0.005%, the mercury removal efficiency hardly increased. The higher the HCl volume fraction, the decline trend after the adsorbent reached the highest mercury removal efficiency became more obvious. This is because in an oxygen-free environment, when the concentration of HCl is high, the surface oxygen of the adsorbent is not enough to support the conversion of HCl and the remaining HCl will compete with Hg^0 for adsorption, covering some active sites on the surface [20], resulting in the overall mercury removal efficiency decreasing relatively quickly. Furthermore, the mercury removal performance improved slightly. Therefore, in an oxygen-free environment, adding a small amount of HCl can promote 1M1C-1 mercury removal, but adding more HCl cannot play a better role.

$$Mn^{4+}(s) + O^{2-}(ad) + HCl(g) \rightarrow Mn^{3+}(s) + OH^{-}(ad) + Cl(ad) \quad (6)$$

$$Hg^0(ad) + Cl(ad) \rightarrow HgCl(ad) \quad (7)$$

$$HgCl(ad) + Cl(ad) \rightarrow HgCl_2(ad) \quad (8)$$

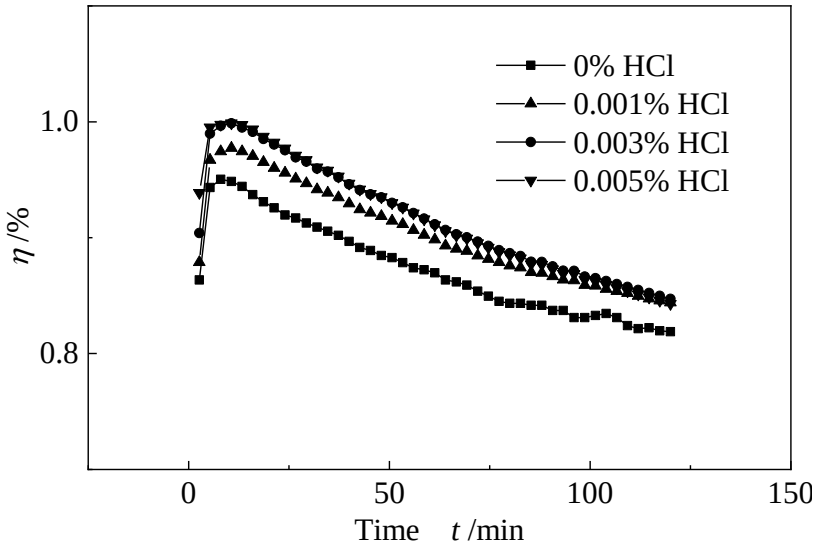

Figure 12. Effect of HCl on the mercury removal efficiency of 1M1C-1.

3.3. Comparison of Performance between Mn-Co-Fe Spinel and Other Adsorbents

Table 1 compares the Hg^0 capture performance and specific saturation magnetization of the 1M1C-1 adsorbent with those of other reported magnetic adsorbents. The capacity of the 1M1C-1 adsorbent for Hg^0 capture was 178.5 μg/g at 150 °C with the Hg^0 removal efficiency of 87.5%, and the specific saturation magnetization was 41 emu/g. This Hg^0 removal performance is basically at the best level among iron-based spinels, which was significantly higher than the Mn–Fe spinel and Fe–Ti–Mn spinel, and only slightly lower than the modified Fe–Ti spinel. It was also at a relatively good level among the magnetically modified natural mineral adsorbent, which was significantly higher than 1M1Atp and 0.2Fe1ATT, and only inferior to 5%CuMAtp. In addition, the specific saturation magnetization of 1M1C-1 was significantly better than the other adsorbents, which means that it

will be easier to magnetically separate it. In general, 1M1C-1 had the best performance in capturing Hg^0 from flue gas and then recovering it by magnetic separation.

Table 1. Comparison of the adsorption capacity and specific saturation magnetization between 1M1C-1 and other adsorbents.

Adsorbents	Adsorption Capacity (μg/g)	Temperature (°C)	Specific Saturation Magnetization (emu/g)	Reference
1M1Atp	70.15	150	29.45	[2]
0.2Fe1ATT	56.7	150	29.5	[12]
Mn–Fe spinel	33	60	37.1	[13]
Modified Fe-Ti spinel	192.6	100	24.6	[10]
5%CuMAtp	307.8	150	18.19	[29]
Fe–Ti–Mn spinel	75	60	29.6	[11]
1M1C-1	178.5	150	41	this work

3.4. Regeneration and Reuse of Spent Mn–Co–Fe Spinel

At present, the most commonly used adsorbent regeneration method is the direct thermal desorption method. According to the literature [13], for the actual flue gas of coal-fired power plants, the optimum temperature for thermal desorption regeneration of the Mn–Fe spinel cannot be lower than 500 °C. In light of the fact that the adsorbent finally screened in this study was calcined at 500 °C for 4 h, and the XRD results also showed that the sample crystal form was single and impurity-free, the adsorbent was regenerated at 500 °C by the direct thermal desorption method, and the mercury adsorption performance test was performed on the adsorbent obtained after regeneration, and the specific test results are shown in Figure 13. As can be seen from the figure, the mercury removal efficiency of the 1M1C-1 adsorbent can be maintained above 85% in the five cycles of regeneration. Therefore, the 1M1C-1 adsorbent had good recycling and regeneration performance.

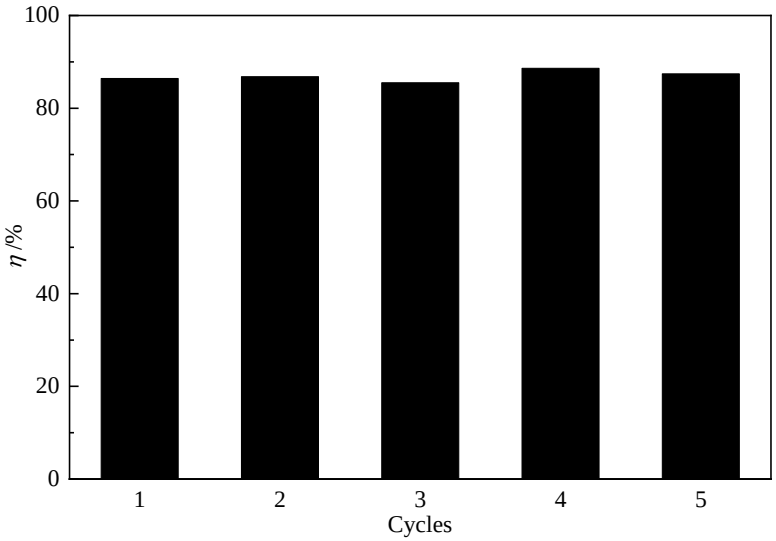

Figure 13. Regeneration performance of 1M1C-1 over five cycles.

4. Conclusions

In this study, a manganese-doped manganese–cobalt–iron spinel adsorbent was prepared by the sol–gel self-combustion method. The sample characterization results and mercury removal performance experiments showed that the synthesized product was the best when the molar ratio of Mn was 0.5. It had a single-phase spinel structure and good magnetic separation performance (41 emu/g), and the mercury removal performance was also relatively good. The average mercury removal efficiency within 120 min was

87.5%; and the Mn doping amount was maintained at 0.5. In the rich combustion, stoichiometric, and lean-burn system, the $Mn_{0.5}Co_{0.5}Fe_2O_4$ spinel was prepared, respectively. The results showed that the synthesized products were all single-phase spinel structures. However, the stoichiometric ratio system was most conducive to product synthesis, and the resulting product had the most excellent mercury removal performance. Within the experimental temperature, the mercury removal ability of 1M1C-1 was relatively good, and it gradually increased with the increase in temperature. However, physical adsorption was dominant at lower temperature, while physical adsorption was inhibited and mercury desorption occurred at a higher temperature. In this case, only moderate temperature, physical adsorption, and chemical adsorption work together to play an important role in the range. O_2 can promote the mercury removal performance of 1M1C-1. However, 10% O_2 was enough to regenerate the lattice oxygen or chemisorption oxygen consumed on the surface, and the higher O_2 volume fraction had little further effect on the mercury removal performance. The addition of different volume fractions of SO_2 has an inhibitory effect on the mercury removal of 1M1C-1, and the higher the volume fraction, the more obvious the inhibitory effect. The main reason is that SO_2 competes with Hg^0 for adsorption, and there may be side reactions that weaken the mercury removal capacity of the adsorbent. The addition of a small amount of HCl can promote 1M1C-1 mercury removal, but the addition of more HCl does not have a better promotion effect. This is mainly due to the insufficient surface oxygen of the adsorbent in an oxygen-free environment to support more HCl conversion, and the remaining HCl will instead begin competitive adsorption with Hg^0, covering part of the active sites on the surface, and weakening the active chlorine atom's promotion of mercury removal from the adsorbent. Compared with other reported adsorbents, the 1M1C-1 adsorbent had the best performance for Hg^0 capture from flue gas and then recovering it by magnetic separation. In addition, it also had a strong recycling performance, and the mercury removal efficiency could be maintained above 85% in five cycles after thermal desorption regeneration at 500 °C.

Author Contributions: This work presented here was carried out with collaboration among all authors. Methodology, J.H., Z.Z. and Y.X. (Yueyang Xu); validation, J.H. and Y.X. (Yuanqiang Xu); formal analysis, J.H.; investigation, J.H. and Y.X. (Yuanqiang Xu); data curation, J.H.; writing—original draft preparation, J.H.; writing—review and editing, Z.Z.; funding acquisition and supervision, Y.X. (Yueyang Xu). All authors have read and agreed to the published version of the manuscript.

Funding: The project was supported by the National Key Research and Development Program of China (2017YFC0210203) and Science and Technology Innovation Project of CHN Energy (GJNY-20-109).

Institutional Review Board Statement: Not applicable.

Informed Consent Statement: Not applicable.

Data Availability Statement: The data presented in this study are available on request from the corresponding author.

Conflicts of Interest: The authors declare no conflict of interest.

References

1. Xu, Y.L.; Zhong, Q.; Liu, X.Y. Elemental mercury oxidation and adsorption on magnesite powder modified by Mn at low temperature. *J. Hazard. Mater.* **2015**, *283*, 252–259. [CrossRef] [PubMed]
2. Chen, H.; Huang, Y.J.; Dong, L.; Cao, J.H.; Xia, Z.P.; Qin, W.H. Study on the preparation of magnetic attapulgite and its mercury removal performance. *J. Fuel Chem. Technol.* **2018**, *46*, 1392–1400.
3. Yang, Y.J.; Liu, J.; Zang, B.K.; Liu, F. Density functional theory study on the heterogeneous reaction between Hg^0 and HCl over spinel-type $MnFe_2O_4$. *Chem. Eng. J.* **2017**, *308*, 897–903. [CrossRef]
4. Wang, J.W.; Xu, C.; Qin, W.; Zang, J.L.; Zang, X.L.; Dong, Y.J.; Cui, X.F. Hg^0 removal by palygorskite (PG) supported MnO_x catalyst. *J. Fuel Chem. Technol.* **2020**, *48*, 1442–1451. [CrossRef]
5. Zhang, A.C.; Zheng, W.W.; Song, J.; Hu, S.; Liu, Z.C.; Xiang, J. Cobalt manganese oxides modified titania catalysts for oxidation of elemental mercury at low flue gas temperature. *Chem. Eng. J.* **2014**, *236*, 29–38. [CrossRef]
6. Liu, F.F.; Zhang, J.Y.; Zhao, Y.C.; Zheng, C.G. Mercury removal from flue gas by metal oxide-loaded attapulgite mineral sorbent. *Combust. Sci. Technol.* **2014**, *20*, 553–557.

7. Sun, Q.K.; Huang, Y.J.; Wang, L.; Guan, Z.W.; Li, M.; Zhou, J.; Wang, Y. Experimental study on mercury removal efficiencies of magnetic Fe_3O_4-Ag composite nanoparticles. *Chem. Ind. Eng. Prog.* **2017**, *36*, 1101–1106.
8. Ma, Y.P.; Xu, T.F.; Wang, J.D.; Shi, Y.R.; Wang, H.Y.; Xiong, F.G.; Xu, H.M.; Ma, Y.X.; Zhang, H.Z. Superior Hg^0 capture performance and SO_2 resistance of Co-Mn binary metal oxide-modified layered MCM-22 zeolite for SO_2-containing flue gas. *Environ. Sci. Pollut. Res. Int.* **2021**, *28*, 16447–16457. [CrossRef]
9. Chen, L.; Liu, S.Y.; Lv, W.Y.; Yang, K.; Li, Y. Effect of Manganese loading on zero valent mercury adsorption on magnetic iron oxides. *Environ. Eng.* **2019**, *37*, 131–137.
10. Zou, S.J.; Liao, Y.; Xiong, S.C.; Huang, N.; Geng, Y.; Yang, S.J. H_2S-modified Fe-Ti spinel: A recyclable magnetic sorbent for recovering gaseous elemental mercury from flue gas as a co-benefit of wet electrostatic precipitators. *Environ. Sci. Technol.* **2017**, *51*, 3426–3434. [CrossRef]
11. Liao, Y.; Xiong, S.C.; Dang, H.; Xiao, X.; Yang, S.J.; Wong, P.K. The centralized control of elemental mercury emission from the flue gas by a magnetic rengenerable Fe-Ti-Mn spinel. *J. Hazard. Mater.* **2015**, *299*, 740–746. [CrossRef] [PubMed]
12. Dong, L.; Huang, Y.J.; Chen, H.; Liu, L.Q.; Liu, C.Q.; Xu, L.G.; Zha, J.R.; Wang, Y.X.; Liu, H. Magnetic γ-Fe_2O_3-loaded attapulgite sorbent for Hg^0 removal in coal-fired flue gas. *Energy Fuels* **2019**, *33*, 7522–7533. [CrossRef]
13. Dang, H. *The Centralized Control of Elemental Mercury Emission from the Flue Gas Using Magnetic Mn-Fe Spinel*; Nanjing University of Science & Technology: Nanjing, China, 2017.
14. Xiong, S.C.; Xiao, X.; Huang, N.; Dang, H.; Liao, Y.; Zou, S.J.; Yang, S.J. Elemental mercury oxidation over Fe-Ti-Mn spinel: Performance, mechanism, and reaction kinetics. *Environ. Sci. Technol.* **2017**, *51*, 531–539. [CrossRef] [PubMed]
15. Cai, J.; Shen, B.X.; Li, Z.; Chen, J.H.; He, C. Removal of elemental mercury by clays impregnated with KI and KBr. *Chem. Eng. J.* **2014**, *241*, 19–27. [CrossRef]
16. Liu, H.; Yang, J.P.; Tian, C.; Zhao, Y.C.; Zhang, J.Y. Mercury removal from coal combustion flue gas by modified palygorskite adsorbents. *Appl. Clay Sci.* **2017**, *147*, 36–43. [CrossRef]
17. Zhang, Y.S.; Duan, W.; Liu, Z.; Cao, Y. Effects of modified fly ash on mercury adsorption ability in an entrained-flow reactor. *Fuel* **2014**, *128*, 274–280. [CrossRef]
18. Yang, Y.J.; Zhang, B.H.; Liu, J.; Wang, Z.; Miao, S. Mercury removal by recyclable and regenerable $Cu_xMn_{(3-x)}O_4$ spinel-type sorbents. *Combust. Sci. Technol.* **2017**, *23*, 511–515.
19. Dong, L.; Huang, Y.J.; Yuan, Q.; Cheng, H.Q.; Ding, S.Y.; Wang, S.; Duan, Y.F. Experimental study on the mercury removal from flue gas using manganese modified titanium-zirconium and titanium-tin composite oxide catalysts. *J. Fuel Chem. Technol.* **2020**, *48*, 741–751.
20. Wang, Z.; Yang, Y.J.; Liu, J.; Liu, F.; Yan, X.C. Experimental and theoretical insights into the effect of syngas components on Hg^0 removal over $CoMn_2O_4$ sorbent. *Ind. Eng. Chem. Res.* **2020**, *59*, 8078–8085. [CrossRef]
21. Shi, D.L.; Lu, Y.; Tang, Z.; Han, F.N.; Chen, R.Y.; Xu, Q. Removal of elemental mercury from simulated flue gas by cerium oxide modified attapulgite. *Korean J. Chem. Eng.* **2014**, *31*, 1405–1412. [CrossRef]
22. He, C.; Shen, B.X.; Chen, J.H.; Cai, J. Adsorption and oxidation of elemental mercury over Ce-MnO_x/Ti-PILCs. *Environ. Sci. Technol.* **2014**, *48*, 7891–7898. [CrossRef]
23. Xie, Y.J.; Yan, B.; Tian, C.; Liu, Y.X.; Liu, Q.X.; Zeng, H.B. Efficient removal of elemental mercury (Hg^0) by SBA-15-Ag adsorbents. *J. Mater. Chem. A* **2014**, *2*, 17730–17734. [CrossRef]
24. Cimino, S.; Scala, F. Removal of elemental mercury by MnO_x catalysts supported on TiO_2 or Al_2O_3. *Ind. Eng. Chem. Res.* **2015**, *55*, 5133–5138. [CrossRef]
25. Liu, H.; You, Z.W.; Yang, S.; Liu, C.; Xie, X.F.; Xiang, K.S.; Wang, X.Y.; Yan, X. High-efficient adsorption and removal of elemental mercury from smelting flue gas by cobalt sulfide. *Environ. Sci. Pollut. Res.* **2019**, *26*, 6735–6744. [CrossRef] [PubMed]
26. Li, H.L.; Zhu, L.; Wang, J.; Li, L.Q.; Shih, K. Development of nano-sulfide sorbent for efficient removal of elemental mercury from coal combustion fuel gas. *Environ. Sci. Technol.* **2016**, *50*, 9551–9557. [CrossRef] [PubMed]
27. Kong, L.N.; Zou, S.J.; Mei, J.; Geng, Y.; Zhao, H.; Yang, S.J. Outstanding resistance of H_2S-modified Cu/TiO_2 to SO_2 for capturing gaseous Hg^0 from nonferrous metal smelting flue gas: Performance and reaction mechanism. *Environ. Sci. Technol.* **2018**, *52*, 10003–10010. [CrossRef]
28. Liu, W.; Xu, H.M.; Liao, Y.; Quan, Z.W.; Li, S.C.; Zhao, S.J.; Qu, Z.; Yan, N.Q. Recyclable CuS sorbent with large mercury adsorption capacity in the presence of SO_2 from non-ferrous metal smelting flue gas. *Fuel* **2019**, *235*, 847–854. [CrossRef]
29. Ding, S.Y.; Huang, Y.J.; Chen, H.; Dong, L.; Fan, C.H.; Hu, H.J.; Qi, E.B. Mercury removal performance of $CuCl_2$-modified magentic attapulgite. *Chem. Ind. Eng. Prog.* **2020**, *39*, 1187–1195.
30. Yang, J.P.; Zhao, Y.C.; Zhang, J.Y.; Zheng, C.G. Regenerable cobalt oxide loaded magnetosphere catalyst from fly ash for mercury removal in coal combustion flue gas. *Environ. Sci. Technol.* **2014**, *48*, 14837–14843. [CrossRef]
31. Zhang, Z.J.; Wang, Z.L.; Chakoumakos, B.C.; Yin, J.S. Temperature dependence of cation distribution and oxidation state in magnetic Mn-Fe ferrite nanocrystals. *J. Am. Chem. Soc.* **1998**, *120*, 1800–1804. [CrossRef]
32. Chandel, M.; Ghosh, B.K.; Moitra, D.; Patra, M.K.; Vadera, S.R.; Ghosh, N.N. Synthesis of various ferrite (MFe_2O_4) nanoparticles and their application as efficient and magnetically separable catalyst for biginelli reaction. *J. Nanosci. Nanotechnol.* **2018**, *18*, 2481–2492. [CrossRef] [PubMed]
33. Wang, Y.X.; Huang, Y.J.; Dong, L.; Yuan, Q.; Ding, S.Y.; Cheng, H.Q.; Wang, S.; Duan, Y.F. Experimental study on mercury removal of coal-fired flue gas over Co-doped iron-based oxide sorbent. *J. Fuel Chem. Technol.* **2020**, *48*, 785–794.

34. Shi, Y.J.; Deng, S.; Wang, H.M.; Huang, J.Y.; Li, Y.K.; Zhang, F.; Shu, X.Q. Fe and Co modified vanadium-titanium steel slag as sorbents for elemental mercury adsorption. *RSC. Adv.* **2016**, *6*, 15999–16009. [CrossRef]
35. Yue, Z.X.; Zhou, J.; Zhang, H.G.; Gui, Z.L.; Li, L.T. Auto-combustion behavior of nitrate-citrate gels and synthesis of ferrite nano-particles. *J. Chin. Ceram. Soc.* **1999**, *27*, 84–88.
36. Guo, M.Y.; Wang, Y.M.; Pan, Z.D.; Liu, S. Synthesis of nanocrystalline $(Co_{0.5}Cu_{0.5})(MnFe)O_4$ ceramic pigment via solution combustion technique. *J. Chin. Ceram. Soc.* **2015**, *43*, 411–417.
37. Yang, Y.J.; Liu, J.; Zhang, B.K.; Liu, F. Mechanistic studies of mercury adsorption and oxidation by oxygen over spinel-type $MnFe_2O_4$. *J. Hazard. Mater.* **2017**, *321*, 154–161. [CrossRef]
38. Xu, Y.; Luo, G.Q.; Pang, Q.C.; He, S.W.; Deng, F.F.; Xu, Y.Q.; Yao, H. Adsorption and catalytic oxidation of elemental mercury over regenerable magnetic Fe-Ce mixed oxides modified by non-thermal plasma treatment. *Chem. Eng. J.* **2019**, *358*, 1454–1463. [CrossRef]
39. Dong, L.; Huang, Y.J.; Liu, L.Q.; Liu, C.Q.; Xu, L.G.; Zha, J.R.; Chen, H.; Liu, H. Investigation of elemental mercury removal from coal-fired boiler flue gas over MIL101-Cr. *Energy Fuels* **2019**, *33*, 8864–8875. [CrossRef]
40. Zhang, Z.; Wu, J.; Li, B.; Xu, H.B.; Liu, D.J. Removal of elemental mercury from simulated flue gas by ZSM-5 modified with Mn-Fe mixed oxides. *Chem. Eng. J.* **2019**, *375*, 121946. [CrossRef]
41. Yang, S.J.; Yan, N.Q.; Guo, Y.F.; Wu, D.Q.; He, H.P.; Qu, Z.; Li, J.F.; Zhou, Q.; Jia, J.P. Gaseous elemental mercury capture from flue gas using magnetic nanosized $(Fe_{3-x}Mn_x)_{1-\delta}O_4$. *Environ. Sci. Technol.* **2011**, *45*, 1540–1546. [CrossRef]